Quantum Monte Carlo simulation study of free energies and melting transitions in Coulomb solids

Hiroshi Iyetomi, Shuji Ogata, and Setsuo Ichimaru
Department of Physics, University of Tokyo, Bunkyo-ku, Tokyo 113, Japan
(Received 13 July 1992; revised manuscript received 21 December 1992)

The free energy of a one-component plasma (OCP) in a bcc crystalline state is calculated by a quantum Monte Carlo (MC) simulation method. The partition function in a Feynman path-integral form is sampled over a semiclassical reference system of 128 MC particles, with quantum fluctuations generated according to the Wigner-Seitz model. Exchange effects are shown to be negligible. Helmholtz-free energies of the Coulomb solid, computed at 48 combinations of density and temperature parameters, are decomposed into harmonic and anharmonic contributions and are fitted to analytic formulas; accuracy of the result is confirmed through comparison with the Wigner-Kirkwood expansions and with the ground-state results. The free-energy formulas are applied for calculation of the melting curves in dense carbon and helium OCP materials, appropriate to interiors of degenerate stars, showing that the melting curves start to deviate from the classical predictions at around $\rho_m = 2\times 10^8$ g/cm^3 (C) and 2×10^3 g/cm^3 (He), far lower than the values predicted by analyses of the Lindemann type.

I. INTRODUCTION

Equations of state for dense plasmas have attracted the interest of many investigators as fundamental issues in condensed matter physics, with important applications to dense stellar materials,[1] such as those found in the interiors of white dwarfs and crustal matter of neutron stars. Accurate knowledge on the thermodynamic properties of the dense plasmas is indispensable for the analyses of internal structures and evolution of those degenerate stars.[2,3]

A one-component plasma (OCP), a basic model for such dense stellar matter, consists of identical particles with charge Ze embedded in a rigid uniform background of neutralizing charges.[1] For a classical OCP either in a fluid or in a solid state, Monte Carlo (MC) simulation studies have precisely determined the thermodynamic functions such as the free energies.[4–8] The Wigner-Kirkwood expansion calculation, combined with classical simulation results, has extended our knowledge up to the terms on the order of $\hbar^4$ in the quantum corrections.[9] The properties of the OCP in a bcc-crystalline ground state have been calculated in the framework of lattice dynamics,[6,10–12] followed by a variational calculation.[13] For the quantum OCP fluids such as electrons and spin-zero bosons, a variational approach with trial wave functions was used for evaluation of the ground-state energies.[13,14] Furthermore, we mention a direct Green's-function Monte Carlo calculation performed for the electron systems.[15] The equation of state for quantum OCPs at arbitrary temperatures has remained as an outstanding problem, however, since interplay between the thermal and quantum effects introduces an additional complication. Recently the free energies of quantum electron liquids at arbitrary temperatures have been approached by the integral equation methods.[1,16]

Once accurate equations of state for the OCP are obtained, one can determine the fluid-solid transition (Wigner transition) by finding an intersection between free energies in these two states. The melting conditions for the classical OCP have now been well established owing to analyses through the MC simulations.[7,8,17,18] Quantum effects may enter the melting-transition criteria for such light nuclei as He and C found in degenerate stars. Early attempts to investigate such quantum effects include the calculation of the equations of state for dense plasmas due to Lamb and Van Horn.[19] These authors evaluated the free energy of the solid OCP within the harmonic approximation, and took into account the leading quantum correction to the classical free energy in the fluid state. The melting curves for the various OCPs were thereby constructed. Nagara, Nagata, and Nakamura[17] developed a reduced-moment expansion method to partially sum up infinite numbers of the quantum correction terms and studied the melting transition in the OCP.

Mochkovitch and Hansen[20] adopted a different approach based on a generalized Lindemann criterion. These authors showed that the Lindemann parameter for the OCP took on significantly different values in the classical and quantum limits, and thereby devised an interpolation scheme for the Lindemann parameter at arbitrary temperatures. Although the scheme has merit in that the melting curves can be approached with information in the solid state alone, a drawback is that basically it cannot surpass the Lindemann phenomenology.

In this paper we present quantum Monte Carlo (QMC) calculations of the free energies in OCP solids based on the path-integral formulation.[21] The calculations enable one to bridge accurately the known asymptotic results in the semiclassical and ground-state limits.[9,11,13] We then address ourselves to the quantum effects on the fluid-solid transition in the OCP along the line initiated by Lamb and Van Horn, but now taking additional account of anharmonic effects in the solid and of the second-order quantum correction to the free energy in the fluid.

In Sec. II, a path-integral formulation suitable for the free-energy calculation is described. We introduce a

reference system which takes into account major parts of the correlation properties of Coulomb solids; deviations of the free energy from these reference values are thereby computed. In Sec. III, the Wigner-Kirkwood expansion results for OCPs in fluid as well as in solid states are revisited, and ground-state properties of OCP solids are summarized. The numerical results are presented in Sec. IV. Accuracy of the calculations is confirmed through comparison of the results with the limiting calculations in the semiclassical regime and at zero temperature. In Sec. V, anharmonic contribution to the free energy is isolated from its harmonic contribution and both contributions are fitted accurately to analytic formulas which satisfy the boundary conditions in the semiclassical and quantum limits. Section VI is devoted to an application of the obtained formulas; the melting curves in carbon and helium OCPs are calculated. The principal results are summarized in Sec. VII.

II. PATH-INTEGRAL FORMULATION FOR THE FREE ENERGY

When the plasma obeys the classical statistics, its state in equilibrium at temperature T and number density n is characterized by a single Coulomb-coupling parameter, defined as

$$\Gamma=\beta(Ze)^2/a \ . \tag{1}$$

Here $a=(3/4\pi n)^{1/3}$ is the ion-sphere radius and β is the inverse temperature in energy units. Quantum effects in the fluid plasma are measured by the ratio between the thermal de Broglie wavelength and the ion-sphere radius, that is,

$$\Lambda=\frac{\hbar\sqrt{2\pi\beta}}{a\sqrt{M}} \ , \tag{2}$$

where M is the mass of a plasma particle. An alternative parameter Y, more appropriate to solid plasmas, is given as

$$Y=\beta\hbar\omega_0=\beta\hbar\sqrt{4\pi(Ze)^2n/3M} \ , \tag{3}$$

where ω_0 is the Einstein frequency in the Wigner-Seitz model of a Coulomb solid. A quantum plasma at zero temperature is described in terms of the usual dimensionless density parameter,

$$R_S=aM(Ze)^2/\hbar^2 \ . \tag{4}$$

Among these parameters, two are independent; they are mutually related via

$$\Lambda=\sqrt{2\pi\Gamma/R_S} \ , \tag{5}$$

$$Y=\Gamma/\sqrt{R_S} \ . \tag{6}$$

Path-integral formulation of the quantum mechanics due to Feynman[21] enables one to express the partition function Ξ for the OCP solid with the interaction potential V as

$$\Xi=\int d\bar{x}\int_{x(0)=x(\beta\hbar)}Dx(u)\exp\left[-\frac{1}{\hbar}\int_0^{\beta\hbar}du\,H[x(u)]\right] \ , \tag{7}$$

where

$$\bar{x}=\frac{1}{\beta\hbar}\int_0^{\beta\hbar}du\,x(u) \ , \tag{8}$$

$$H[x(u)]=\frac{M}{2}\left[\frac{\partial x(u)}{\partial u}\right]^2+V[x(u)] \ , \tag{9}$$

and $x=\{\mathbf{r}_1,\mathbf{r}_2,\ldots,\mathbf{r}_N\}$ represents a set of the particle coordinates. The path $x(u)$ in Eq. (7) is a periodic function of an "imaginary time" u with periodicity $\beta\hbar$, and the path integral is carried out over the whole periodic paths with a given "time average," $\bar{x}$, defined by Eq. (8).

Difficulties in a direct computation of the partition function even for classical systems have been well documented.[22] The Metropolis algorithm,[23] a powerful method for importance sampling, does not work for the partition function itself. A way of calculating the partition function is thus to introduce a reference system, with known properties, which has a potential $V_{\rm ref}[x(u)]$, so that

$$H_{\rm ref}[x(u)]=\frac{M}{2}\left[\frac{\partial x(u)}{\partial u}\right]^2+V_{\rm ref}[x(u)] \ . \tag{10}$$

The partition function Ξ and hence the Helmholtz free-energy F can be expressed in terms of the corresponding quantities of the reference system as

$$\Xi=\Xi_{\rm ref}\langle\exp[-\beta\overline{\Delta V}]\rangle_{\rm ref} \ , \tag{11}$$

$$\Delta F\equiv F-F_{\rm ref}=-\frac{1}{\beta}\ln[\langle\exp[-\beta\overline{\Delta V}]\rangle_{\rm ref}] \ , \tag{12}$$

$$\overline{\Delta V}=\frac{1}{\beta\hbar}\int_0^{\beta\hbar}du\{V[x(u)]-V_{\rm ref}[x(u)]\} \ , \tag{13}$$

where $\langle A\rangle_{\rm ref}$ refers to the ensemble average in the reference system:

$$\langle A\rangle_{\rm ref}=\frac{1}{\Xi_{\rm ref}}\int d\bar{x}\int_{x(0)=x(\beta\hbar)}Dx(u)\,A\exp\left[-\frac{1}{\hbar}\int_0^{\beta\hbar}du\,H_{\rm ref}[x(u)]\right] \ . \tag{14}$$

The efficiency of computation depends on accuracy of the adopted reference system in mimicking the original system. Here we take the following system based on the Wigner-Seitz model:

$$V_{\rm ref}[x(u)]=V(\bar{x})+\frac{M}{2}\omega_0^2[x(u)-\bar{x}]^2 \ . \tag{15}$$

The first term on the right-hand side of Eq. (15) corre-

sponds to the classical approximation, and the second term represents a harmonic interaction of plasma particles with the Wigner-Seitz spheres. The reference free-energy $F_{\rm ref}$ can then be calculated as

$$f_{\rm ref}\equiv\frac{\beta F_{\rm ref}}{N}=f_{\rm CL}+3\ln\left[\frac{\sinh(Y/2)}{Y/2}\right], \tag{16}$$

where $f_{\rm CL}$ is the free energy of the classical OCP solid per particle in temperature units. The advantage in the present choice for $V_{\rm ref}$ may be appreciated through the ability of Eq. (16) in reproducing the leading term in the quantum corrections, given by Eq. (22) below, as well as the classical free energy. Equation (16) also yields the energy of zero-point oscillation, which is only 13% larger than the correct value [see Eq. (29) below] for the quantum OCP solid.

To execute the path-integral computations in practice we approximately replace the continuous path $x(u)$ by a discrete path with P segments (Trotter decomposition),

$$x(u)\cong\{x(0),x(1),\ldots,x(P)=x(0)\}, \tag{17}$$

and thereby establish the isomorphism between quantum and classical systems:[24] One looks upon each quantum particle with coordinate $\mathbf{r}_i$ as a classical polymer chain consisting of P atoms with coordinate $\{\mathbf{r}_i(1),\mathbf{r}_i(2),\ldots,\mathbf{r}_i(P)\}$. The polymers in the equivalent classical system interact with each other in a way as depicted in Fig. 1(a). The classical system corresponding to the reference quantum system with Eq. (15) is also exhibited in Fig. 1(b). The Trotter theorem[25] guarantees that the statistical properties of the classical polymer chain asymptotically approach those of a quantum particle as P increases.

The multidimensional integration in Eq. (14) can be carried out by a Monte Carlo sampling method. The numerical complexities involved in the computation are reduced by utilizing the Fourier representation[21,26] for $x(n)$ $(n=0,1,\ldots,P-1)$,

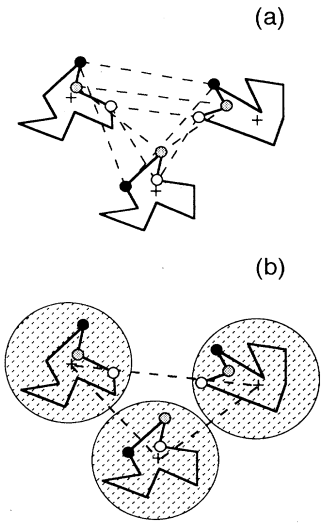

FIG. 1. Schematic pictures for the equivalent classical systems corresponding to the quantum OCP (a) and the reference quantum system (b) based on the Wigner-Seitz model. The dashed lines in (a) refer to reduced Coulomb potentials, $(Ze)^2/rP$, between the specific atoms (depicted by circles with the same filling patterns) in polymers. The crosses and shaded circles in (b) denote the centroid and the associated Wigner-Seitz sphere for each polymer; the dashed lines refer to the full Coulomb potentials, $(Ze)^2/r$, between the centroids.

$$x(n)=\bar{x}+\sum_{k=1}^{P/2-1}a_k\cos\left[\frac{2\pi nk}{P}\right]+\frac{(-1)^n}{2}a_{P/2}+\sum_{k=1}^{P/2-1}b_k\sin\left[\frac{2\pi nk}{P}\right]. \tag{18}$$

Equation (14) is then rewritten as

$$\langle A\rangle_{\rm ref}=\frac{J}{\Xi_{\rm ref}}\int d\bar{x}\exp[-\beta V(\bar{x})]\prod_{j=1}^{P/2}\int_{-\infty}^{\infty}da_j\prod_{j=1}^{P/2-1}\int_{-\infty}^{\infty}db_j\,A\exp\left[-\sum_{k=1}^{P/2}\frac{1}{2}\left[\frac{a_k}{\sigma_k}\right]^2-\sum_{k=1}^{P/2-1}\frac{1}{2}\left[\frac{b_k}{\sigma_k}\right]^2\right], \tag{19}$$

with

$$\sigma_k^2=(1+\delta_{k,P/2})\left[\frac{P^2M}{\beta\hbar^2}\left[1-\cos\frac{2\pi k}{P}\right]+\frac{1}{2}\beta M\omega_0^2\right]^{-1}. \tag{20}$$

The Jacobian J in Eq. (19) arises from transformation of the variables between the real and Fourier spaces; it plays no part in the calculation of ensemble averages. The multidimensional sampling is thus performed independently with respect to the variables of integration. The centroid $\bar{x}$ is sampled with the classical Boltzmann weight, and the Fourier coefficients, $\{a_k\}$ and $\{b_k\}$, are generated according to independent Gaussian distributions with standard deviations σ_k.

III. SEMICLASSICAL AND GROUND-STATE RESULTS

The free energy is expressed by the Wigner-Kirkwood expansion[27] in powers of $\hbar^2$ as

$$f\equiv\frac{\beta F}{N}=f^{(0)}+f^{(1)}+f^{(2)}+\cdots. \tag{21}$$

Here $f^{(0)}$ is the free energy of the classical OCP. The

accurate-fitting formulas for $f^{(0)}$ based on the MC simulations are available both in the fluid and solid states.[7,8] The quantum corrections are given by

$$f^{(1)}=\frac{\Gamma\Lambda^2}{16\pi}\ , \tag{22}$$

$$f^{(2)}=-\frac{\Gamma^2\Lambda^4}{3840\pi^2}[12J(\Gamma)+9K(\Gamma)+1]\ , \tag{23}$$

where

$$J(\Gamma)=\frac{a^6}{3N}\left\langle\sum_{i\neq j}^{N}\frac{1}{r_{ij}^6}\right\rangle\ , \tag{24}$$

$$K(\Gamma)=\frac{a^6}{9N}\left\langle\sum_{i\neq j\neq k}^{N}3\frac{(\mathbf{r}_{ij}\cdot\mathbf{r}_{ik})^2}{r_{ij}^5r_{ik}^5}-\frac{1}{r_{ij}^3r_{ik}^3}\right\rangle\ , \tag{25}$$

and $r_{ij}=|\mathbf{r}_{ij}|=|\mathbf{r}_i-\mathbf{r}_j|$.

Hansen and Vieillefosse[9] have evaluated $J(\Gamma)$ and $K(\Gamma)$ using the radial distribution functions for the classical OCPs obtained by MC simulation with $N=128$ and 250; the three-body distribution function required in the evaluation of $K(\Gamma)$ was replaced by the Kirkwood superposition formula. They also provided analytic formulas for $J(\Gamma)$ both in the fluid and solid states, and found that $K(\Gamma)$ could be approximated with the value for a perfect bcc lattice over the whole range of Γ.

To confirm their results we have repeated the calculations on the basis of the MC simulations with much larger number of particles, $N=1458$; we have directly evaluated $K(\Gamma)$ without the use of the Kirkwood approximation for ternary distribution functions. Figures 2 and 3 show good agreement between the present results and those of Hansen and Vieillefosse in both phases.

The free energy of the OCP solid consists of three parts: the bcc Madelung-energy term, the harmonic, and anharmonic contributions, i.e.,

$$f=-0.895\,929\,\Gamma+f_{\rm HM}+f_{\rm AH}\ . \tag{26}$$

The results for $f_{\rm HM}$ and $f_{\rm AH}$ in the Wigner-Kirkwood expansion are given explicitly as

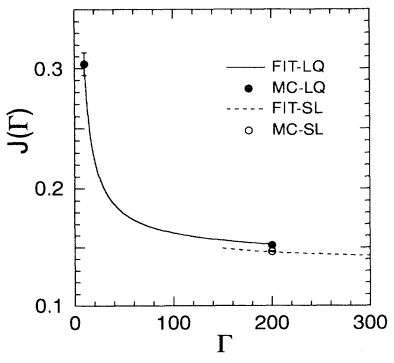

FIG. 2. The function $J(\Gamma)$ in the second-order quantum correction term. The solid and open circles are the MC values for the OCP in the fluid and solid states, respectively. The solid and dashed curves refer to the fitting results[9] for the fluid and solid OCP.

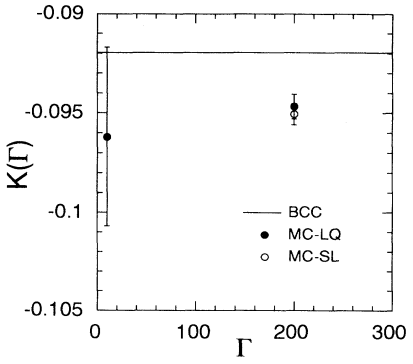

FIG. 3. The function $K(\Gamma)$ in the second-order quantum correction term. The solid and open circles are the MC values for the OCP in the fluid and solid states, respectively. The solid line refers to the value for the perfect bcc lattice.[9]

$$f_{\rm HM}^{\rm SCL}=-0.845\,88+3\ln Y+\frac{Y^2}{8}-1.9038\times10^{-3}Y^4\ , \tag{27}$$

$$f_{\rm AH}^{\rm SCL}=-\left(\frac{10.84}{\Gamma}+\frac{176.4}{\Gamma^2}+\frac{5.980\times10^4}{\Gamma^3}\right)-\frac{Y^4}{80}\left(\frac{1.2993}{\Gamma}+\frac{61.252}{\Gamma^2}\right)\ . \tag{28}$$

The first three terms on the right-hand side of Eq. (28) refers to the classical anharmonic contribution obtained by Dubin[18] through fitting to the MC results. Recently Nagara, Nagata, and Nakamura[17] and Dubin[18] have revisited the previous fitting analysis[7] to find that the critical Γ value for melting in the classical OCP slightly decreased from $\Gamma=178$ to $\Gamma=172$.

The ground-state energy ($T\to0$) of a quantum OCP solid with bcc symmetry has been evaluated by Carr, Coldwell-Horsfall, and Fein[11] as

$$f_{\rm HM}^{\rm QM}=\frac{1.328\,6\Gamma}{\sqrt{R_S}}\ , \tag{29}$$

$$f_{\rm AH}^{\rm QM}=-\frac{0.365\Gamma}{R_S}\ . \tag{30}$$

The harmonic (zero-point oscillation) contribution $f_{\rm HM}^{\rm QM}$ was obtained through a normal-mode analysis; we cited there the refined value due to Pollock and Hansen.[6] The anharmonic contribution $f_{\rm AH}^{\rm QM}$ arises from a first-order perturbation due to quartic terms in the displacements and from a second-order perturbation due to cubic terms. Ceperley[13] later confirmed the perturbational result, Eq. (30), through a variational calculation with a spherical trial function. The exchange effects on the ground-state energy of an electron solid were also estimated by Carr, Coldwell-Horsfall, and Fein,[11] adopting an antisymmetric wave function of independent oscillators, which were arranged in an antiferromagnetic way on the bcc-lattice sites. It has thereby been shown that the calculat-

ed exchange term, vanishing exponentially with increase of R_S, is completely negligible near the freezing point,[15] $R_S \cong 100$, as compared with Eq. (30). We expect that the same conclusion is applicable to the exchange effects in boson solids.

IV. QMC SIMULATION RESULTS

The QMC simulations are performed for the OCP solids in a bcc-crystalline state for 48 parametric combinations of Γ and Y as shown in Fig. 4, where the classical and quantum melting lines, given[17,18] by $\Gamma \cong 172$ and estimated[15] as $R_S \cong 160$ (zero-spin bosons), are added for reference purposes. The cases thus cover the classical as well as quantum melting regimes. The cubic simulation cell with periodic boundary conditions contains 128 particles. The Ewald summation technique is used to handle the long-range nature of the Coulomb potential. The fitting formula[7] of the Ewald potential in polynomials significantly reduces the computation time. The quantum fluctuations of the particles are treated with 20 atoms in each classical polymer chain. For calculation of the free-energy difference Δf, Eq. (12) has been expanded in cumulants and the result has been terminated at the second order, i.e.,

$$\Delta f \cong \frac{1}{N}\langle \beta \overline{\Delta V} \rangle_{\rm ref} - \frac{1}{2N}\left\langle (\beta \overline{\Delta V} - \langle \beta \overline{\Delta V} \rangle_{\rm ref})^2 \right\rangle_{\rm ref} . \quad (31)$$

We have generated 4000 statistically independent configurations to calculate the ensemble averages in Eq. (31). Convergence both in the Trotter decomposition and in the cumulant expansion will be discussed later.

Since the simulations are performed for systems with finite size, the computed results may contain extra dependence on the number N of the particles used. To quench such an N dependence we have adopted the center-of-mass correction scheme[8] for the Δf, that is,

$$\Delta f = \frac{N}{N-1}\Delta f_{\rm QMC} + \frac{3}{N-1}\ln\left[\frac{\sinh(Y/2)}{Y/2}\right] , \quad (32)$$

where $\Delta f_{\rm QMC}$ denotes the original difference in the free energies. The scheme thus consists in multiplying the variational part (sum of the harmonic and anharmonic contributions) in the free energy by a factor $N/(N-1)$. The effectiveness of such a center-of-mass correction has been demonstrated for the classical OCP solids.[8]

Figure 5 shows the QMC results for Δf with and without the center-of-mass corrections as a function of Y at various Γ values. The same figure also includes the asymptotic results, $\Delta f_{\rm SCL}$ and $\Delta f_{\rm QM}$, in the semiclassical and quantum regimes; these are defined as

$$\Delta f_{\rm SCL} = -0.895\,929\Gamma + f_{\rm HM}^{\rm SCL} + f_{\rm AH}^{\rm SCL} - f_{\rm ref} , \quad (33)$$

$$\Delta f_{\rm QM} = -0.895\,929\Gamma + f_{\rm HM}^{\rm QM} + f_{\rm AH}^{\rm QM} - f_{\rm ref} . \quad (34)$$

We first remark that the center-of-mass correction plays an important role in the semiclassical regime, where the extra Y^2 dependence involved in the raw data are removed in the corrected values. The leading quantum correction in Eq. (33) is of the order of Y^4, since the Y^2 term in $f_{\rm HM}^{\rm SCL}$ is exactly canceled by the corresponding term in $f_{\rm ref}$. We thus see that this cancellation is preserved by the center-of-mass correction procedure in Eq. (32). As Fig. 5 shows clearly, the simulation results approach the zero-temperature calculations almost independent of Γ, as Y increases beyond approximately 5. This trend demonstrates adequacy of the choice, $P=20$, in the treatment of quantum fluctuations even at the largest value, $Y=40$. Excellent agreement between the nu-

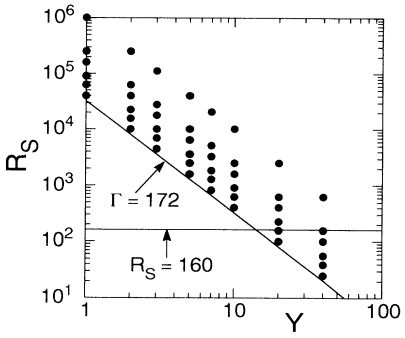

FIG. 4. Diagram depicting the 48 parametric combinations in the Y-R_s plane where the quantum MC simulations have been performed.

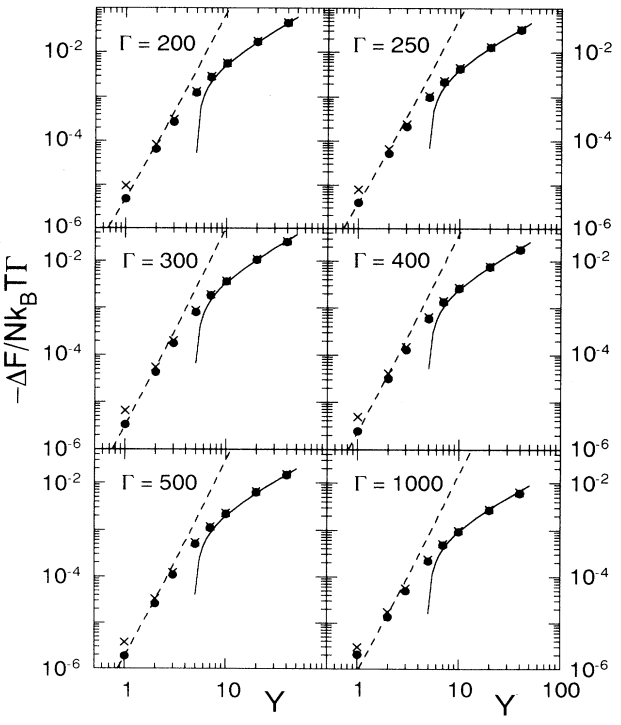

FIG. 5. Negative of the deviation ΔF for the free energy from the reference value in units of $N\Gamma\beta^{-1}$. The solid circles and crosses are the QMC values with and without the center-of-mass corrections, respectively. The dashed and solid curves refer to the semiclassical and ground-state results, respectively.

TABLE I. QMC results for $-\beta\Delta F/N\Gamma$ with the center-of-mass correction. The numbers in parentheses denote the standard errors in the last digits of the means over 4000 configuration averages.

	Γ					
Y	200	250	300	400	500	1000
1	$4.8(3)\times10^{-6}$	$4.0(3)\times10^{-6}$	$3.3(2)\times10^{-6}$	$2.4(2)\times10^{-6}$	$1.9(1)\times10^{-6}$	$2.06(6)\times10^{-6}$
2	$6.5(2)\times10^{-5}$	$5.2(1)\times10^{-5}$	$4.3(1)\times10^{-5}$	$3.15(9)\times10^{-5}$	$2.58(7)\times10^{-5}$	$1.35(3)\times10^{-5}$
3	0.000 267(6)	0.000 212(5)	0.000 174(4)	0.000 129(3)	0.000 107(3)	$5.0(1)\times10^{-5}$
5	0.001 24(3)	0.000 98(2)	0.000 80(2)	0.000 59(1)	0.000 49(1)	0.000 217(5)
7	0.002 76(6)	0.002 17(5)	0.001 78(4)	0.001 31(3)	0.001 09(3)	0.000 48(1)
10	0.005 5(1)	0.0043(1)	0.003 53(8)	0.002 58(6)	0.002 17(5)	0.000 93(2)
20	0.0169(4)	0.0129(3)	0.0103(2)	0.0074(2)	0.0062(1)	0.002 65(6)
40	0.046(1)	0.0324(8)	0.0251(6)	0.0173(4)	0.0144(3)	0.0060(1)

merical and asymptotic results in the respective limits guarantees validity and accuracy of the second-order cumulant approximation adopted for Δf. As an independent check, we have calculated the third- and fourth-order cumulants and found no significant contributions from those higher-order terms.

We finally list all the results for Δf obtained in the present simulations and the estimated standard errors in Table I. In the error estimates, we have assumed that the statistical fluctuations involved in the average and variance of $\overline{\Delta V}$ are mutually independent.

V. ANHARMONIC CONTRIBUTION

The accuracy achieved in the present simulations enables us to extract the anharmonic contributions $f_{\rm AH}$ from the QMC results for Δf given in the previous section. Combining Eqs. (12) and (26) we calculate $f_{\rm AH}$ as

$$f_{\rm AH}=f_{\rm ref}+\Delta f+0.895\,929\,\Gamma-f_{\rm HM}\ . \tag{35}$$

The harmonic contributions $f_{\rm HM}$ were tabulated by Pollock and Hansen[6] as a function of Y. The extracted results for $f_{\rm AH}$ with the statistical errors are shown in Fig. 6 for all the Γ values at which the simulations have been done. The good agreement between the QMC and asymptotic results are again manifested, except at $\Gamma=1000$. The anharmonic contributions are so small at such a large Γ that their evaluations are hindered by the statistical uncertainties.

Accurate analytic formulas for $f_{\rm HM}$ and $f_{\rm AH}$ are useful for the purposes of applications. To obtain such formulas, we consider a model Hamiltonian for an Einstein oscillator with an additional quartic term representing anharmonicity:

$$H_E=\frac{\mathbf{p}^2}{2M}+\frac{M}{2}\omega^2\mathbf{x}^2-l(x^4+y^4+z^4)\ , \tag{36}$$

where $\mathbf{p}$ and $\mathbf{x}=(x,y,z)$ denote three-dimensional momentum and coordinate of the oscillating particle. The harmonic and anharmonic contributions to the free energy in such a model are calculated as

$$f^E_{\rm HM}=3\ln\left[2\sinh\left[\frac{\beta\hbar\omega}{2}\right]\right]\ , \tag{37}$$

$$f^E_{\rm AH}=-\frac{9}{4}\beta l\left[\frac{\hbar}{M\omega}\right]^2\coth^2\left[\frac{\beta\hbar\omega}{2}\right]\ , \tag{38}$$

where we have adopted the first-order perturbational calculation for $f^E_{\rm AH}$ in the anharmonic interaction.

Regarding the harmonic frequency ω and the anharmonic-coupling strength l in Eqs. (37) and (38) as fitting parameters, we have obtained the following analytic formulas for $f_{\rm HM}$ and $f_{\rm AH}$. The harmonic term takes a form

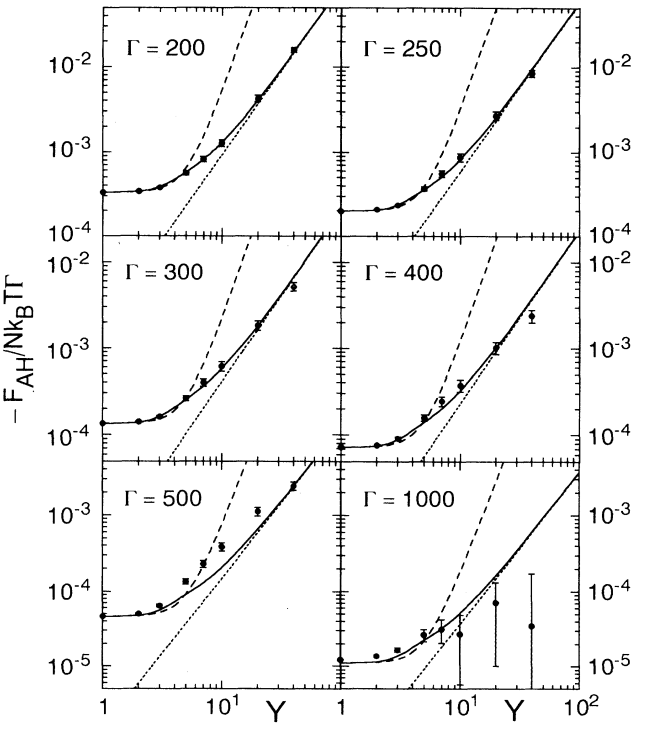

FIG. 6. Negative of the anharmonic contribution $F_{\rm AH}$ in units of $N\Gamma\beta^{-1}$. The circles are the quantum MC values with standard errors depicted by the vertical bars. The solid curves are the fitted results. The dashed and dotted curves refer to the semiclassical and ground-state results, respectively.

$$f_{\rm HM}=3\ln\left[2\sinh\left[\frac{Y}{2}g(Y)\right]\right], \tag{39}$$

with

$$g(Y)=\frac{0.7543+0.092\,45Y^2+0.003\,386\,Y^4}{1+0.104\,6Y^2+0.003\,823\,Y^4}. \tag{40}$$

For the anharmonic term, we replace ω in Eq. (38) with the Einstein frequency ω_0 and thereby simplify the resulting formula, so that

$$f_{\rm AH}=-\tfrac{9}{4}L(\xi,Y)Y\coth^2(Y/2), \tag{41}$$

where

$$L(\xi,Y)=\frac{\Gamma Y\{P(\xi)-0.081\,67P(\xi)Y^2+Q(\xi)Y^4\}}{1+0.085Y^2+R(\xi)Y^6}. \tag{42}$$

A new parameter ξ has been introduced in Eq. (41),

$$\xi=\Gamma\tanh(8.5/Y)=\sqrt{R_S}\,Y\tanh(8.5/Y), \tag{43}$$

which reduces to the Coulomb-coupling parameters relevantly both in the classical and quantum limits:

$$\lim_{Y\to 0}\xi=\Gamma,\quad \lim_{Y\to\infty}\xi=8.5\sqrt{R_S}. \tag{44}$$

The fitting functions, $P(\xi)$, $Q(\xi)$, and $R(\xi)$, in Eq. (42) have been parametrized as

$$P(\xi)=1.204/\xi^2+19.60/\xi^3+6.644\times10^3/\xi^4, \tag{45}$$

$$Q(\xi)=0.001\,805/\xi^2+0.085\,07/\xi^3+0.009\,444P(\xi), \tag{46}$$

$$R(\xi)=0.085\,32\xi^2Q(\xi). \tag{47}$$

The semiclassical and ground-state results, Eqs. (27), (28), (29), and (30), are built into formulas (39) and (41) through the parametrization of $g(Y)$, $P(\xi)$, $Q(\xi)$, and $R(\xi)$. Comparison between the fitted and original values for $f_{\rm HM}$ shows that the errors in Eq. (39) are confined to 0.04%. The fitted results for $f_{\rm AH}$ based on Eq. (41) are included in Fig. 6. We see that Eq. (41) reproduces the simulation results within the statistical uncertainties for $\Gamma\le400$, where the reliable QMC results are available.

One can derive the equation of state and other thermodynamic quantities from the fitting formulas (39) and (41) through standard thermodynamic relations. As an example, Fig. 7 displays the anharmonic contribution $S_{\rm AH}$ to the entropy as a function of Y at $\Gamma=200$, 300, and 500. The minimum, separating the classical and quantum regimes, is located around $Y=4$ for each curve, regardless of the Γ values. The small hump observed in $f_{\rm AH}$ (see Fig. 6) gives rise to such a transit behavior in $S_{\rm AH}$. Harmonic and anharmonic contributions to the entropy are also compared in Fig. 7. The magnitude of the anharmonic contribution is relatively small except in the quantum regime of $Y>10$.

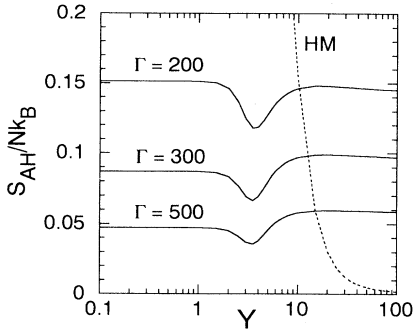

FIG. 7. The anharmonic contributions (solid curves) in the entropy as a function of Y for various Γ, compared with the harmonic contribution (dotted curve).

VI. QUANTUM EFFECTS ON THE MELTING

As an application of formulas (39) and (41), we examine the fluid-solid transition in dense carbon or helium OCP materials relevant to the interiors of white dwarf stars. It is expected that solid cores may be formed during cooling of those stars.

Quantum effects of ions in the solid phase have been fully taken into account through the use of Eqs. (39) and (41). For the free energy of a fluid OCP, on the other hand, we use the Wigner-Kirkwood expansion results, Eq. (21), up to the terms on the order of $\hbar^4$; the treatments here are basically semiclassical. Hence we may be justified to treat only that part of melting which is caused by the thermal motion of particles.

We thus construct the melting curves with the OCP fluid equations of state at different degrees of quantum corrections: the zeroth-order expression (WK0) with $f^{(0)}$ alone, the first-order expression (WK1) with $f^{(0)}+f^{(1)}$, and the second-order expression (WK2) with $f^{(0)}+f^{(1)}+f^{(2)}$. The results so calculated for C and He plasmas are shown in Figs. 8 and 9, respectively, where also drawn for comparison are the melting line, $\Gamma=172$, in the classical OCP and the two lines, $\Lambda=1$ and $Y=1$, measuring extents of the quantum effects involved. These calculations clearly demonstrate sensitive dependence of the transition curve on the treatment of the ionic quantum effects.

The WK0 calculations imply that the ionic quantum effects in the solid phase depress its stability. Inclusion of the leading quantum correction Eq. (22) to the classical free energy, which is a positive quantity, acts to enlarge the domain of the solid phase even over a purely classical prediction, as shown in the WK1 result. We remark that the WK1 calculation with omission of the anharmonic term in the solid free energy is essentially equivalent to that carried out by Lamb and Van Horn.[19]

The second-order quantum correction Eq. (23), included in the WK2 scheme, is negative definite and hence tends to destabilize the solid phase. The departures of the resulting transition curves from the classical ones are magnified in the insets of Figs. 8 and 9. Since the leading quantum corrections are identical in both phases, the behavior of the melting curve near the classical regime is

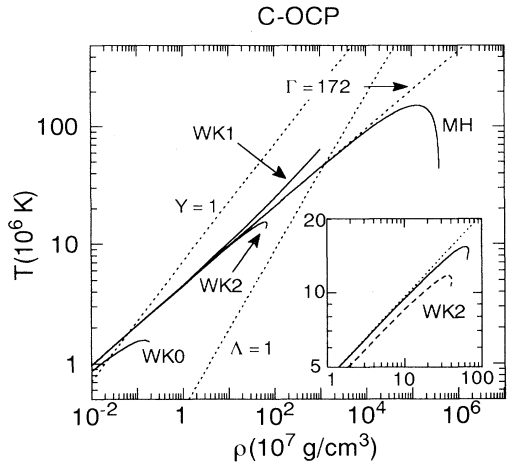

FIG. 8. Melting curves for a carbon OCP in various schemes. The Wigner-Kirkwood expansion terms in the free energy for the fluid OCP are systematically taken into account: WK0 refers to the melting curve obtained with the classical term only; WK1, that with the leading (first-order) quantum correction in addition to the classical term; WK2, with the terms up to the order of $\hbar^4$. The curve designated as MH represents the calculation based on the Mochkovitch-Hansen scheme (Ref. 20). The inset magnifies the departure of the melting curve from the classical condition (dotted line) based on the second-order calculation (WK2—solid curve); the melting curve obtained without the anharmonic term in the solid free energy is also included (dashed curve).

determined by a delicate balance between the quantum corrections of the second and higher order in the two phases. To assess the anharmonic effects on the melting, we have repeated the WK2 calculations, but with the harmonic term alone; the results are also shown in the insets of Figs. 8 and 9 by dashed lines. The anharmonicity enhances stability of the solid phase by 10–20% in the temperature. The WK2 calculation gives the most accurate result in the present treatments. The strong bending observed in the melting curves based on the WK2 scheme implies breakdown of the approximations.

The average mass density ρ in carbon white dwarfs usually takes[2] on a value in 10^5–10^8 g/cm^3. For a white dwarf with accretion from a companion star, which is regarded as a progenitor of the type-I supernova, the relevant range of the mass density is extended[28] up to $\rho=10^{10}$ g/cm^3. According to the WK2 calculation, the quantum effects begin to change the classical melting line beyond $\rho=2\times10^8$ g/cm^3 in the C plasma. The evolution of the accreting white dwarfs and the mechanism of the subsequent explosions may therefore be influenced by the quantum effects as reflected in the melting.

This result contrasts with that of Mochkovitch and Hansen (MH) based on a generalized (Y dependent) Lindemann criterion.[20] Through such calculations these authors arrived at a conclusion that the melting was completely classical below $\rho=4\times10^{11}$ g/cm^3. Figure 8 incorporates the transition curve calculated in the MH scheme, but with fitting parameters so modified as to reproduce the classical melting condition, $\Gamma=172$. The modification decreases the critical mass density at which the quantum effects begin to emerge to 5×10^{10} g/cm^3, which is still much larger than the present result. The overestimation of the critical mass density by the MH scheme is also manifested for the He OCP as shown in Fig. 9; the critical mass densities are predicted at 2×10^3 g/cm^3 and 7×10^5 g/cm^3 in the present and MH calculations, respectively. We remark in passing that the considerable difference between the two predictions may be ascribed to improper treatment of the $\hbar^4$-correction term in the interpolation formula for the Lindemann parameter in the MH scheme. Nagara, Nagata, and Nakamura[17] also obtained the critical mass densities considerably lower than the MH values; their results are 2×10^9 g/cm^3 and 3×10^4 g/cm^3 for C and He OCPs, respectively.

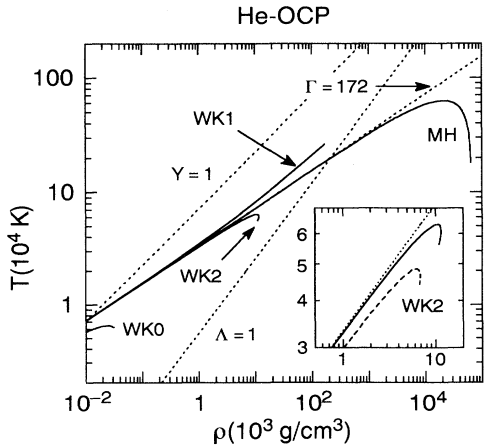

FIG. 9. Same as in Fig. 8, but for a helium OCP.

VII. CONCLUSION

We have calculated the Helmholtz free energy for the Coulomb bcc solid using the quantum Monte Carlo method. The partition function was represented in a Feynman path-integral form with no account of the exchange effects, and a semiclassical system with the associated Wigner-Seitz sphere for each particle was adopted as a reference system. The deviation of the free energy from the reference value was thereby computed in a wide range of density and temperature with 128 MC particles. The excellent agreement between the simulation results and the asymptotic calculations in the semiclassical and quantum regimes has established the accuracy of the simulations. We then decomposed the numerical results into the harmonic and anharmonic contributions, each of which was fitted to an analytic form reproducing both the semiclassical and the ground-state results.

As an application of the formulas so obtained, we calculated melting curves in carbon and helium plasmas cor-

responding to the interiors of white dwarfs. The quantum corrections to the classical free energy of the fluid OCP were systematically taken into account to the order of $\hbar^4$. The results demonstrate sensitive dependence of the transition curves on the treatment of quantum properties of ions in the fluid state. The best result in the present calculations predicts the critical mass densities, $\rho=2\times10^8$ g/cm^3 for C OCP and 2×10^3 g/cm^3 for He OCP, at which the deviations from the classical melting lines become significant; the values are far smaller than those expected in the analyses based on the generalized Lindemann criteria.

ACKNOWLEDGMENTS

This work was supported in part by the Ministry of Education, Science, and Culture through Research Grant Nos. 04455010 and 1387. This research was carried out also as a part of activities through the Japan-U.S. Cooperative Science Program: *Phase Transitions in Dense Astrophysical Plasmas,* supported jointly by the Japan Society for the Promotion of Science and the U.S. National Science Foundation. The authors thank Professor H. M. Van Horn for collaboration and useful discussions on these and related subjects through the program.

[1]S. Ichimaru, H. Iyetomi, and S. Tanaka, Phys. Rep. **149**, 91 (1987).
[2]S. L. Shapiro and S. A. Teukolsky, *Black Holes, White Dwarfs, and Neutron Stars* (Wiley, New York, 1983).
[3]H. M. Van Horn, Science **252**, 384 (1991).
[4]S. G. Brush, H. L. Sahlin, and E. Teller, J. Chem. Phys. **45**, 2102 (1966).
[5]J. P. Hansen, Phys. Rev. A **8**, 3096 (1973).
[6]E. L. Pollock and J.-P. Hansen, Phys. Rev. A **8**, 3110 (1973).
[7]W. L. Slattery, G. D. Doolen, and H. E. DeWitt, Phys. Rev. A **26**, 2255 (1982).
[8]S. Ogata and S. Ichimaru, Phys. Rev. A **36**, 5451 (1987).
[9]J. P. Hansen and P. Vieillefosse, Phys. Lett. **53A**, 187 (1975).
[10]W. J. Carr, Jr., Phys. Rev. **122**, 1437 (1961).
[11]W. J. Carr, Jr., R. A. Coldwell-Horsfall, and A. E. Fein, Phys. Rev. **124**, 747 (1961).
[12]A. A. Kugler, Ann. Phys. (N.Y.) **53**, 133 (1969).
[13]D. Ceperley, Phys. Rev. B **18**, 3126 (1978).
[14]J.-P. Hansen and R. Mazighi, Phys. Rev. A **18**, 1282 (1978).
[15]D. M. Ceperley and B. J. Alder, Phys. Rev. Lett. **45**, 566 (1980).
[16]S. Tanaka and S. Ichimaru, J. Phys. Soc. Jpn. **55**, 2278 (1986).
[17]H. Nagara, Y. Nagata, and T. Nakamura, Phys. Rev. A **36**, 1859 (1987).
[18]D. H. E. Dubin, Phys. Rev. A **42**, 4972 (1990).
[19]D. Q. Lamb and H. M. Van Horn, Astrophys. J. **200**, 306 (1975).
[20]R. Mochkovitch and J.-P. Hansen, Phys. Lett. **73A**, 35 (1979).
[21]R. P. Feynman and A. R. Hibbs, *Quantum Mechanics and Path Integral* (McGraw-Hill, New York, 1965).
[22]D. Frenkel, in *Molecular-Dynamics Simulation of Statistical-Mechanical Systems,* Proceedings of the International School of Physics "Enrico Fermi", Course 97, Varenna, Italy, 1985, edited by G. Ciccotti and W. G. Hoover (North-Holland, Amsterdam, 1986), p. 151.
[23]N. A. Metropolis, A. W. Rosenbluth, M. N. Rosenbluth, A. H. Teller, and E. Teller, J. Chem. Phys. **21**, 1087 (1953).
[24]D. Chandler and P. G. Wolynes, J. Chem. Phys. **74**, 4078 (1981).
[25]H. Trotter, Proc. Am. Math. Soc. **10**, 545 (1959).
[26]D. L. Freeman and J. D. Doll, J. Chem. Phys. **80**, 5709 (1984).
[27]L. D. Landau and E. M. Lifshitz, *Statistical Physics* (Pergamon, New York, 1980).
[28]K. Nomoto, Astrophys. J. **253**, 798 (1982).